Journal of Zhejiang University-SCIENCE C (Computers & Electronics)
ISSN 1869-1951 (Print); ISSN 1869-196X (Online)
www.zju.edu.cn/jzus; www.springerlink.com
E-mail: jzus@zju.edu.cn

Composite disturbance attenuation based saturated control for maintenance of low Earth orbit (LEO) formations*

Jian-cheng FANG[1,2], Ke SUN[†‡1,2]

([1]National Key Laboratory of Inertial Technology, Beihang University, Beijing 100191, China)

([2]Novel Inertial Instrument & Navigation System Technology Key Laboratory of Fundamental Science for National Defense, Beihang University, Beijing 100191, China)

[†]E-mail: kekeesun81@aspe.buaa.edu.cn

Received Nov. 28, 2011; Revision accepted Feb. 23, 2012; Crosschecked Apr. 9, 2012

Abstract: Maintenance of high performance formation control is important for low Earth orbit (LEO) formation missions of small spacecraft. In this paper, a model of nonlinear relative motion dynamics is built, and then nonlinear and important perturbations affecting the formation configuration, such as J_2 and atmospheric drag, are analyzed as disturbances. Global navigation satellite system based relative positioning with nonlinear filtering is adopted to provide state information associated with the perturbations. By combining disturbance observer based control with H_∞ state feedback, a composite disturbance attenuation controller is proposed for maintenance of continuous and accurate formation. With consideration of precise control relying on micro thrusters, a composite disturbance attenuation based saturated controller is designed and its stability is proved. Finally, through numerical simulations, we demonstrate that control accuracy is improved after effectively avoiding perturbations and that stabilization can be satisfied using this method.

Key words: Formation maintenance, Perturbation, Disturbance attenuation, H_∞ state feedback, Saturated control
doi:10.1631/jzus.C1100350 **Document code:** A **CLC number:** V529.1; TP13

1 Introduction

The technology of low Earth orbit (LEO) precise formations of small spacecraft has become increasingly accepted for its application to space-based collaborative missions, such as interferometric synthetic aperture radar (InSAR) measurement, distributed in-situ space exploration, and even cooperative attack and interception (You *et al.*, 2005). The problem of maintaining control of formation configurations is regarded as critical to the long-term effectiveness of such missions.

For a formation system, the relative motion dynamics is the primary problem affecting configuration control and has been studied by many researchers. The linear model based on the Hill-Clohessy-Wiltshire equations is the most widely employed model because of its advantages (Clohessy and Wiltshire, 1960), but it results in a number of errors. Therefore, several forms of nonlinear models have been adopted to improve the situation (Vaddi *et al.*, 2003). Even so, issues relating to space perturbations can have a severe impact on the model. The nonlinearity of differential gravitational acceleration, Earth oblateness, and atmospheric drag are commonly considered the most important perturbations affecting the ideal solutions. Several methods have been proposed to eliminate the influences of perturbations. An approximate quadratic nonlinear model and the influence of secular terms have been studied by Xu and Wang (2008). Canuto *et al.* (2011) have achieved good quantitative relationships between J_2 and the formation distance, altitude, and actuator sizing.

‡ Corresponding author
* Project supported by the National High-Tech R & D Program (863) of China (No. 2008AA12A216) and the National Basic Research Program (973) of China (No. 2009CB72400101C)

Linear J_2 and atmosphere drag have been discussed by Zhang *et al.* (2009). They obtained good solutions but still with errors when simplifying perturbation models. Alfriend *et al.* (2000) and Wnuk and Golebiewska (2007) derived very complex nonlinear perturbations, but these are not convenient for applications in engineering.

High performance and real-time relative navigation are also important as they can provide essential relative state information for the control system. In particular, some states are associated with perturbations. Global navigation satellite system (GNSS) technology is quite mature for spacecraft single-point navigation, and various filters have been presented to improve navigation performance (Yoon and Lundberg, 2001; Fang and Gong, 2010). Recently, this kind of technology has been generalized for formation relative navigation and has achieved considerable success (Winternitz *et al.*, 2009; Buist *et al.*, 2011), but it is still troubled by the nonlinearity of the state equations, and system and measurement noises. For cooperative space missions, formations usually need purpose built designs, such as along-track-follow, fly-around, or Pendulum (Zhang YL *et al.*, 2008; Zhang JX *et al.*, 2009). Obviously, stability of the configuration determines the tasks' long-term effectiveness. Therefore, designing a controller with high precision and robustness is critical for the maintenance of formation configuration, and avoidance of perturbations is the key step. Wang and Zhang (2007) designed a sliding mode control for formation maintenance, mainly against J_2 perturbations. Massioni *et al.* (2011) designed an H_∞ robust control for configuration stability and Schaub *et al.* (2000) and Zhang *et al.* (2009) adopted a mean orbital element nonlinear feedback control for avoiding the effects of perturbations. But some treatments for perturbations are not yet precise enough, and even partially uncertain perturbations are dealt with as known. Thus, the important perturbations need to be analyzed discriminately and estimated accurately as disturbances to the ideal relative motion model. For disturbance estimation and avoidance, an embedded model control (EMC) was proposed by Canuto (2007), and a disturbance-observer-based control (DOBC) was summarized by Guo *et al.* (2006). The DOBC can estimate exogenous disturbances and modeling errors that can be compensated for through feed-forward. Guo and Chen (2005) presented a DOBC for use in the fields of robot and missile robust control. Furthermore, DOBC has advantages for integration with other conventional controllers (e.g., variable structure and proportional–integral–derivative (PID)) and is less conservative in relation to disturbance types.

The achievement of precise configuration maintenance control requires the support of an advanced micro propulsion system, such as the novel high specific impulse continuous thruster presented by Canuto *et al.* (2011). Thus, the problem of actuator saturation must be balanced in the process of designing the controller.

2 Problem statement and preliminaries

2.1 Coordinate frame and definitions

Before the problem statement, several relevant definitions should be introduced. Relative states among spacecraft are generally expressed in the relative coordinate frame, with its origin O_r coinciding with the master spacecraft's geometric center (see $O_rX_rY_rZ_r$ in Fig. 1), where the X_r axis is along the Earth's radius, Z_r is parallel to the orbital plane normal, and Y_r is tangential to the orbit. This is the same as the master coordinate frame $o_mx_my_mz_m$. Similarly, the slave spacecraft's coordinate frame is $o_sx_sy_sz_s$ and $O_iX_iY_iZ_i$ is the Earth core inertial coordinate frame.

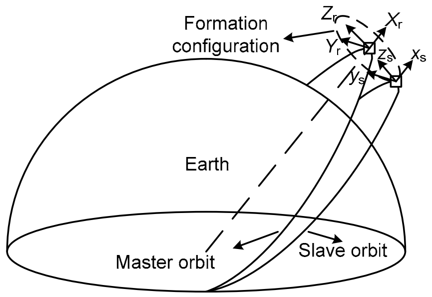

Fig. 1 Coordinate frames for spacecraft formation

Definition 1 (Orbital elements) i_m, f_m, ω_m, and Ω_m represent the master's orbital elements of inclination, true anomaly, argument of perigee, and right ascension of the ascending node (RAAN), respectively; i_s, f_s, ω_s, and Ω_s represent the slave's inclination, true anomaly, argument of perigee, and RAAN, respectively.

Definition 2 (Conversion matrixes) $\boldsymbol{R}_{ri}(i_m, f_m, \omega_m, \Omega_m)$ represents the conversion matrix from the Earth core inertial coordinate frame to the relative coordinate frame; $\boldsymbol{R}_{si}(i_s, f_s, \omega_s, \Omega_s)$ denotes the conversion matrix from the Earth core inertial coordinate frame to the slave coordinate frame; $\boldsymbol{R}_{rs}$ represents the conversion matrix from the slave to the relative coordinate frame. According to the Euler angular algorithm, we know that $\boldsymbol{R}_{rs}=\boldsymbol{R}_{ri}\boldsymbol{R}_{is}=\boldsymbol{R}_{ri}\boldsymbol{R}_{si}^{-1}$.

2.2 Nonlinear relative dynamics modeling and disturbance analysis

For formation configuration maintenance, relative attitudes are not considered in relative states in this paper. Circular orbit formation is discussed here although zero eccentricity is difficult to achieve except under strict orbit control, which is not the case in this paper. Therefore, according to the relative motion between the master and the slaves, the relative dynamics can be described by the following differential equations:

$$\ddot{x} = n^2 x + 2n\dot{y} - \frac{\mu(a_m + x)}{[(a_m + x)^2 + y^2 + z^2]^{3/2}} + \frac{\mu}{a_m^2} + P_{J_2x} + P_{adx} + D_{unx}, \tag{1}$$

$$\ddot{y} = n^2 y - 2n\dot{x} - \frac{\mu y}{[(a_m + x)^2 + y^2 + z^2]^{3/2}} + P_{J_2y} + P_{ady} + D_{uny}, \tag{2}$$

$$\ddot{z} = -\frac{\mu z}{[(a_m + x)^2 + y^2 + z^2]^{3/2}} + P_{J_2z} + P_{adz} + D_{unz}, \tag{3}$$

where x, y, and z are relative positions in the relative coordinate frame, a_m is the master's orbital radius, μ is a gravitational parameter, $n = \sqrt{\mu / a_m^3}$ is the master's mean angular velocity, P_{J_2x}, P_{J_2y}, and P_{J_2z} refer to J_2 perturbations along three axes of the relative coordinate frame, and P_{adx}, P_{ady}, and P_{adz} are atmospheric drag perturbations. D_{unx}, D_{uny}, and D_{unz} represent a combination of other less influential environmental perturbations, such as solar-lunar gravitation, solar radiation pressure, and geomagnetic attraction, which are considered negligible for the LEO close formation in this paper.

To analyze every item of Eqs. (1)–(3) carefully, we need to write them in another form as follows:

$$\begin{aligned}\dot{\boldsymbol{X}} &= [\dot{x} \quad \dot{y} \quad \dot{z} \quad \ddot{x} \quad \ddot{y} \quad \ddot{z}]^{\mathrm{T}} \\ &= \boldsymbol{AX} + \boldsymbol{F} + \boldsymbol{B}_{J_2}\boldsymbol{P}_{J_2} + \boldsymbol{B}_{ad}\boldsymbol{P}_{ad},\end{aligned} \tag{4}$$

$$\boldsymbol{A} = \begin{bmatrix} & 0_{3\times3} & & & \boldsymbol{I}_{3\times3} & \\ n^2 & 0 & 0 & 0 & 2n & 0 \\ 0 & n^2 & 0 & -2n & 0 & 0 \\ 0 & 0 & 0 & 0 & 0 & 0 \end{bmatrix}, \tag{5}$$

$$\boldsymbol{F} = \begin{bmatrix} 0_{3\times1} \\ \dfrac{\mu}{a_m^2} - \dfrac{\mu(a_m + x)}{[(a_m + x)^2 + y^2 + z^2]^{3/2}} \\ -\dfrac{\mu y}{[(a_m + x)^2 + y^2 + z^2]^{3/2}} \\ -\dfrac{\mu z}{[(a_m + x)^2 + y^2 + z^2]^{3/2}} \end{bmatrix}. \tag{6}$$

In Eq. (6), $\mu / [(a_m + x)^2 + y^2 + z^2]^{3/2}$ is the nonlinear term of the differential acceleration $\boldsymbol{F}$. The solution to the differential nonlinear J_2 perturbation is derived from coordinate transformation and differential calculation as follows:

$$\boldsymbol{P}_{J_2} = [P_{J_2x} \quad P_{J_2y} \quad P_{J_2z}]^{\mathrm{T}} = \boldsymbol{R}_{rs}\boldsymbol{P}_{J_2s} - \boldsymbol{P}_{J_2m}, \tag{7}$$

$$\boldsymbol{P}_{J_2m} = \begin{bmatrix} P_{mx} \\ P_{my} \\ P_{mz} \end{bmatrix} = \alpha_m \begin{bmatrix} 1 - 3\sin^2 i_m \sin^2(\omega_m + f_m) \\ \sin^2 i_m \sin(2(\omega_m + f_m)) \\ \sin(2i_m)\sin(\omega_m + f_m) \end{bmatrix}, \tag{8}$$

$$\boldsymbol{P}_{J_2s} = \begin{bmatrix} P_{sx} \\ P_{sy} \\ P_{sz} \end{bmatrix} = \alpha_s \begin{bmatrix} 1 - 3\sin^2 i_s \sin^2(\omega_s + f_s) \\ \sin^2 i_s \sin(2(\omega_s + f_s)) \\ \sin(2i_s)\sin(\omega_s + f_s) \end{bmatrix}, \tag{9}$$

where $\alpha_m = -3\bar{J}_2\mu r_e^2 / (2r_m^4)$, $\alpha_s = -3\bar{J}_2\mu r_e^2 / (2r_s^4)$, $r_m=a_m$, and $r_s=a_s$. $\bar{J}_2$ is the geodynamics form factor, r_e is the mean radius of the Earth, $\boldsymbol{P}_{J_2m}$ and $\boldsymbol{P}_{J_2s}$ are J_2 perturbations to the master and slave in coordinate frames $o_m x_m y_m z_m$ and $o_s x_s y_s z_s$ respectively, and r_s is the slave's orbital radius, which can be expressed as $r_s = \sqrt{(r_m + x)^2 + y^2 + z^2}$ with relative coordinates.

Similar to Eq. (7), the differential air drag perturbation is $\boldsymbol{P}_{ad} = [P_{adx} \quad P_{ady} \quad P_{adz}]^{\mathrm{T}} = \boldsymbol{R}_{rs}\boldsymbol{P}_{ads} - \boldsymbol{P}_{adm}$, where $\boldsymbol{P}_{adm} = \left[P_{admx} \quad C_d\rho s_m\dot{y}_m^2 / (2m_m) \quad P_{admz}\right]^{\mathrm{T}}$ and $\boldsymbol{P}_{ads} = \left[P_{adsx} \quad C_d\rho s_s\dot{y}_s^2 / (2m_s) \quad P_{adsz}\right]^{\mathrm{T}}$ are perturbations on the master and slave in coordinate frames $o_m x_m y_m z_m$ and $o_s x_s y_s z_s$, respectively. C_d is the aerodynamic coefficient, and ρ is the local atmospheric density, considered the same because of the tiny orbital altitude intercept between the master and slaves. $s_{\rm m}$ and $s_{\rm s}$ are their respective windward areas, $m_{\rm m}$ and $m_{\rm s}$ are masses, and $\dot{y}_{\rm m}$ and $\dot{y}_{\rm s}$ are tangential velocities.

Generally speaking, these perturbations would be offset directly in most methods, but inaccurately. On the one hand, real models of perturbations are difficult to describe completely; on the other hand, acquisition of the relative state variables of positions (x, y, z, $\dot{x}$, $\dot{y}$, and $\dot{z}$) and angles ($f_{\rm m}$ and $f_{\rm s}$) associated with perturbations depends on real-time measurement or calculation onboard, which may further introduce errors to the model. Furthermore, some state variables are not easy to measure. For these reasons, a method is proposed to analyze and deal with the nonlinearity and perturbations as disturbances to the ideal relative motion model.

Before the analysis, several reasonable assumptions should be given: the relative states variables have an upper bound; we do not consider the extreme problem of a spacecraft crash.

The Euclidean norm of $\boldsymbol{F}$ is derived into the form

$$\|\boldsymbol{F}\|=\left(\frac{\mu^2}{a_{\rm m}^2+2a_{\rm m}x+l^2}\right.\\ \left.-\frac{2\mu^2(a_{\rm m}+x)}{a_{\rm m}^2(a_{\rm m}^2+2a_{\rm m}x+l^2)^{3/2}}+\frac{\mu^2}{a_{\rm m}^4}\right)^{2/3}, \tag{10}$$

where $l=\sqrt{x^2+y^2+z^2}$ is the distance between the master and slave. Based on the assumption, it can be derived that $\|\boldsymbol{F}\|<W_{\rm F}$, and $W_{\rm F}$ is a positive constant.

According to Eqs. (7)–(9), $\boldsymbol{P}_{J_2}$ contains angle variables, which are difficult to measure and calculate precisely, and sometimes are undetectable. Unlike $\boldsymbol{F}$, $\boldsymbol{P}_{J_2}$ is not only norm bounded but has the feature $\|\dot{\boldsymbol{P}}_{J_2}\|=\left\|\frac{{\rm d}\boldsymbol{P}_{J_2}(x,y,z,f_{\rm m},f_{\rm s})}{{\rm d}t}\right\|<W_{J_2}$. It can be proven that $\boldsymbol{P}_{J_2}$ changes slowly and that W_{J_2} is a positive constant.

Similarly, after ignoring very small differences in drag perturbation to $\dot{x}$ and $\dot{z}$, it can also be derived that $\|\boldsymbol{P}_{\rm ad}\|=\|\boldsymbol{P}_{\rm ad}(\dot{y},f_{\rm m},f_{\rm s})\|<W_{\rm ad}$. $W_{\rm ad}$ is also a known positive constant. To sum up, the perturbations discussed above match the disturbance types of Guo and Chen (2005), so different methods will be used to eliminate these classified perturbation influences as disturbances.

3 GNSS based positioning for obtaining relative state variables

Relative position variables associated with perturbations depend on effective relative navigation methods. Here, we introduce a simple relative navigation method for obtaining variables. This is also the premise of the control system in practical applications. In a GNSS based relative positioning method every spacecraft obtains its own position via a GNSS receiver onboard and receives the positions of others through inter-spacecraft links. With differential calculation and filtering, precise relative position results can be obtained. In this paper, a nonlinear dynamics model as given in Eq. (4) is adopted as the state equation:

$$\boldsymbol{\Gamma}=\dot{\boldsymbol{X}}=\boldsymbol{AX}+\boldsymbol{F}+\boldsymbol{B}_{J_2}\boldsymbol{P}_{J_2}+\boldsymbol{B}_{\rm ad}\boldsymbol{P}_{\rm ad}+\boldsymbol{w}. \tag{11}$$

The observation equation is built as

$$\begin{aligned}\boldsymbol{Z}&=[x\quad y\quad z\quad \dot{x}\quad \dot{y}\quad \dot{z}]^{\rm T}=\boldsymbol{R}_{\rm ri}(\boldsymbol{Z}_{\rm s}-\boldsymbol{Z}_{\rm m})+\boldsymbol{e}_{\rm t}+\boldsymbol{\nu}\\ &=\boldsymbol{R}_{\rm ri}([x_{\rm s}\quad y_{\rm s}\quad z_{\rm s}\quad \dot{x}_{\rm s}\quad \dot{y}_{\rm s}\quad \dot{z}_{\rm s}]^{\rm T}\\ &\quad-[x_{\rm m}\quad y_{\rm m}\quad z_{\rm m}\quad \dot{x}_{\rm m}\quad \dot{y}_{\rm m}\quad \dot{z}_{\rm m}]^{\rm T})+\boldsymbol{e}_{\rm t}+\boldsymbol{\nu},\end{aligned} \tag{12}$$

where $\boldsymbol{Z}_{\rm m}(x_{\rm m},y_{\rm m},z_{\rm m},\dot{x}_{\rm m},\dot{y}_{\rm m},\dot{z}_{\rm m})$ indicates the master's state and $\boldsymbol{Z}_{\rm s}(x_{\rm s},y_{\rm s},z_{\rm s},\dot{x}_{\rm s},\dot{y}_{\rm s},\dot{z}_{\rm s})$ is the slave's state. $\boldsymbol{w}$ is system noise and ν is measuring noise (assumed to be white Gaussian noise). $\boldsymbol{e}_{\rm t}$ is the error caused by delays in state information transmission between spacecraft. Such delays can be confirmed by virtue of an embedded precise synchronous clock and a computer. An extended Kalman filter needs to be designed to improve the navigation performance (Han *et al.*, 2010). Note that whether for navigation (and filtering) or control, we often need to turn the system into discrete-time in practical engineering, but the process and closed-loop framework will be introduced in future work.

4 Composite controller design

4.1 DOBC combined with H_∞ state feedback controller

When the initial orbital elements of the formation configuration are determined, $\boldsymbol{X}_\mathrm{d}$ is assumed as the perfect relative state under the ideal space conditions without perturbations. Combined with Eq. (4), the error equation can be formulated as

$$\dot{\boldsymbol{e}} = \dot{\boldsymbol{X}} - \dot{\boldsymbol{X}}_\mathrm{d} = \boldsymbol{A}\boldsymbol{e} + \boldsymbol{F} - \boldsymbol{F}_\mathrm{d} + \boldsymbol{B}_{J_2}\boldsymbol{P}_{J_2} + \boldsymbol{B}_\mathrm{ad}\boldsymbol{P}_\mathrm{ad} + \boldsymbol{B}_\mathrm{u}\boldsymbol{u}, \tag{13}$$

where $\boldsymbol{e}$ is the relative state error, and $\boldsymbol{u}$ is the composite control input, which consists of DOBC and state feedback control. The coefficient matrixes are $\boldsymbol{B}_{J_2} = \boldsymbol{B}_\mathrm{ad} = \boldsymbol{B}_\mathrm{u} = [0_{3\times3} \quad \boldsymbol{I}_{3\times3}]^\mathrm{T}$.

State feedback control is widely used in some systems. Here, a classical state feedback controller is designed as $\boldsymbol{\tau} = \boldsymbol{K}\boldsymbol{X} - \boldsymbol{K}\boldsymbol{X}_\mathrm{d} = \boldsymbol{K}\boldsymbol{e}$, and $\boldsymbol{K}$ is the control gain needing to be determined.

In Eq. (13), we assume the nonlinear term $\boldsymbol{F}_\mathrm{e} = \boldsymbol{F} - \boldsymbol{F}_\mathrm{d}$. It involves state variables x, y, and z, which can be obtained from the relative navigation results in Section 3. Thus, it will be offset during the controller design.

Perturbation $\boldsymbol{P}_{J_2}$ involves f_m and f_s, except for x, y, and z. Real-time f_m and f_s are considered not easy to obtain precisely, especially for formation on the track. Therefore, $\boldsymbol{P}_{J_2}$ is estimated through subsequent observer design. The observer is formulated as

$$\begin{cases} \dot{\boldsymbol{\gamma}} = -\boldsymbol{L}\boldsymbol{B}_{J_2}\hat{\boldsymbol{P}}_{J_2} - \boldsymbol{L}(\boldsymbol{A}\boldsymbol{X} + \boldsymbol{F}_\mathrm{e} + \boldsymbol{B}_\mathrm{u}\boldsymbol{u}), \\ \hat{\boldsymbol{P}}_{J_2} = \boldsymbol{\gamma} + \boldsymbol{L}\boldsymbol{X}, \end{cases} \tag{14}$$

where $\boldsymbol{L}$ is the observer gain to be designed and the disturbance observer estimation error is designed as $\boldsymbol{e}_{\boldsymbol{P}_{J_2}} = \boldsymbol{P}_{J_2} - \hat{\boldsymbol{P}}_{J_2}$. $\hat{\boldsymbol{P}}_{J_2}$ is the estimation of $\boldsymbol{P}_{J_2}$. Then

$$\dot{\boldsymbol{e}}_{\boldsymbol{P}_{J_2}} = \dot{\boldsymbol{P}}_{J_2} - \boldsymbol{L}\boldsymbol{B}_{J_2}\boldsymbol{e}_{\boldsymbol{P}_{J_2}} - \boldsymbol{L}\boldsymbol{B}_\mathrm{ad}\boldsymbol{P}_\mathrm{ad} \tag{15}$$

and $\boldsymbol{L}$ should be designed appropriately to make $\boldsymbol{e}_{\boldsymbol{P}_{J_2}} \to 0$.

Next, the composite controller is constructed as $\boldsymbol{u} = -\boldsymbol{b}\boldsymbol{F}_e - \hat{\boldsymbol{P}}_{J_2} + \boldsymbol{\tau}$. Denote $\boldsymbol{b} = [0_{3\times3} \quad \boldsymbol{I}_{3\times3}]$. Substituting $\boldsymbol{u}$ in Eq. (13) and combining with Eq. (15), the augmented system is constructed as

$$\begin{bmatrix} \dot{\boldsymbol{e}} \\ \dot{\boldsymbol{e}}_{\boldsymbol{P}_{J_2}} \end{bmatrix} = \begin{bmatrix} \boldsymbol{A} + \boldsymbol{B}_\mathrm{u}\boldsymbol{K} & \boldsymbol{B}_{J_2} \\ 0_{3\times6} & -\boldsymbol{L}\boldsymbol{B}_{J_2} \end{bmatrix} \begin{bmatrix} \boldsymbol{e} \\ \boldsymbol{e}_{\boldsymbol{P}_{J_2}} \end{bmatrix} + \begin{bmatrix} 0_{6\times3} & \boldsymbol{B}_\mathrm{ad} \\ \boldsymbol{I}_{3\times3} & -\boldsymbol{L}\boldsymbol{B}_\mathrm{ad} \end{bmatrix} \begin{bmatrix} \dot{\boldsymbol{P}}_{J_2} \\ \boldsymbol{P}_\mathrm{ad} \end{bmatrix}. \tag{16}$$

The controller $\boldsymbol{u}$ consists of three parts: the first is to offset nonlinear impacts, the second is to estimate and compensate J_2 using a disturbance observer, and the last part is used to attenuate drag disturbance and to control relative position through a state feedback controller. Simultaneously, the state feedback controller needs to satisfy asymptotic stability required by H_∞ performances, which will be proved in the next subsection.

4.2 System stability

Now, the system (16) is proven uniformly ultimately bounded. At the same time, the composite controller gains $\boldsymbol{K}$ and $\boldsymbol{L}$ can be resolved through a series of demonstrations. Adding an output equation to Eq. (16), the new augmented system can be written as

$$\begin{cases} \dot{\bar{\boldsymbol{X}}} = \bar{\boldsymbol{A}}\bar{\boldsymbol{X}} + \bar{\boldsymbol{B}}\boldsymbol{D}, \\ \bar{\boldsymbol{Z}} = \boldsymbol{C}\bar{\boldsymbol{X}}, \end{cases} \tag{17}$$

where

$$\bar{\boldsymbol{X}} = \begin{bmatrix} \boldsymbol{e} \\ \boldsymbol{e}_{\boldsymbol{P}_{J_2}} \end{bmatrix}, \quad \bar{\boldsymbol{A}} = \begin{bmatrix} \boldsymbol{A} + \boldsymbol{B}_\mathrm{u}\boldsymbol{K} & \boldsymbol{B}_{J_2} \\ 0 & -\boldsymbol{L}\boldsymbol{B}_{J_2} \end{bmatrix},$$

$$\bar{\boldsymbol{B}} = \begin{bmatrix} 0 & \boldsymbol{B}_\mathrm{ad} \\ \boldsymbol{I} & -\boldsymbol{L}\boldsymbol{B}_\mathrm{ad} \end{bmatrix}, \quad \boldsymbol{C} = [\boldsymbol{C}_1 \quad \boldsymbol{C}_2], \quad \boldsymbol{D} = \begin{bmatrix} \dot{\boldsymbol{P}}_{J_2} \\ \boldsymbol{P}_\mathrm{ad} \end{bmatrix}.$$

Theorem 1 In the system (17), for a given $\alpha>0$, if there exist $\boldsymbol{Q}_1>0$, $\boldsymbol{P}_2>0$, $\boldsymbol{R}_1$, and $\boldsymbol{R}_2$ satisfying

$$\boldsymbol{\varPi} = \begin{bmatrix} \mathrm{sym}(\boldsymbol{G}) & \boldsymbol{Q}_1\boldsymbol{C}_1^\mathrm{T} & 0 & \boldsymbol{B}_\mathrm{ad} & \boldsymbol{B}_{J_2} \\ \boldsymbol{C}_1\boldsymbol{Q}_1^\mathrm{T} & -\alpha\boldsymbol{I} & 0 & 0 & \boldsymbol{C}_2 \\ 0 & 0 & -\alpha\boldsymbol{I} & 0 & \boldsymbol{P}_2 \\ \boldsymbol{B}_\mathrm{ad}^\mathrm{T} & 0 & 0 & -\alpha\boldsymbol{I} & -\boldsymbol{B}_\mathrm{ad}{}^\mathrm{T}\boldsymbol{R}_2^\mathrm{T} \\ \boldsymbol{B}_{J_2}^\mathrm{T} & \boldsymbol{C}_2^\mathrm{T} & \boldsymbol{P}_2^\mathrm{T} & -\boldsymbol{R}_2\boldsymbol{B}_\mathrm{ad} & -\mathrm{sym}(\boldsymbol{R}_2\boldsymbol{B}_{J_2}) \end{bmatrix} < 0, \tag{18}$$

where $\boldsymbol{G}=\boldsymbol{A}\boldsymbol{Q}_1+\boldsymbol{B}_{\rm u}\boldsymbol{R}_1$, sym($\boldsymbol{Y}$)=$\boldsymbol{Y}$+$\boldsymbol{Y}^{\rm T}$ for a square matrix $\boldsymbol{Y}$, then the system (17) is uniformly ultimately bounded, and satisfies the H_∞ performance index: $\|\bar{\boldsymbol{Z}}\|<\alpha\|\boldsymbol{D}\|$. The controller gain can be obtained as $\boldsymbol{K}=\boldsymbol{R}_1\boldsymbol{Q}_1^{-1}$, $\boldsymbol{L}=\boldsymbol{P}_2^{-1}\boldsymbol{R}_2$.

Proof Based on a bounded real lemma (de Souza and Xie, 1992), we substitute $\bar{\boldsymbol{A}}$, $\bar{\boldsymbol{B}}$, $\boldsymbol{C}$, $\boldsymbol{D}$. After elementary matrix transformation, it is not difficult to derive

$$\boldsymbol{\Pi}_1=\begin{bmatrix}\mathrm{sym}(\boldsymbol{H}) & \boldsymbol{C}_1^{\rm T} & 0 & \boldsymbol{P}_1\boldsymbol{B}_{\rm ad} & \boldsymbol{P}_1\boldsymbol{B}_{J_2}\\ \boldsymbol{C}_1 & -\gamma\boldsymbol{I} & 0 & 0 & \boldsymbol{C}_2\\ 0 & 0 & -\gamma\boldsymbol{I} & 0 & \boldsymbol{P}_2\\ \boldsymbol{B}_{\rm ad}^{\rm T}\boldsymbol{P}_1 & 0 & 0 & -\gamma\boldsymbol{I} & -\boldsymbol{B}_{\rm ad}{}^{\rm T}\boldsymbol{L}^{\rm T}\boldsymbol{P}_2\\ \boldsymbol{B}_{J_2}^{\rm T}\boldsymbol{P}_1 & \boldsymbol{C}_2^{\rm T} & \boldsymbol{P}_2^{\rm T} & -\boldsymbol{P}_2\boldsymbol{L}\boldsymbol{B}_{\rm ad} & \mathrm{sym}(-\boldsymbol{P}_2\boldsymbol{L}\boldsymbol{B}_{J_2})\end{bmatrix}<0, \tag{19}$$

where $\boldsymbol{H}=\boldsymbol{P}_1(\boldsymbol{A}+\boldsymbol{B}_{\rm u}\boldsymbol{L})$, $\boldsymbol{P}_1=\boldsymbol{Q}_1^{-1}$, $\boldsymbol{P}_2=\boldsymbol{Q}_2^{-1}$, $\boldsymbol{R}_1$=$\boldsymbol{K}\boldsymbol{Q}_1$, and $\boldsymbol{R}_2$=$\boldsymbol{P}_2\boldsymbol{L}$. Then pre- and post-multiplying inequality (19) by the diagonal matrix diag{$\boldsymbol{Q}_1$, $\boldsymbol{I}$, $\boldsymbol{I}$, $\boldsymbol{I}$, $\boldsymbol{I}$}, inequality (18) is obtained.

5 Saturated controller and stability

The precision of the micro thruster is satisfied but there is a lack of power when considering high performance configuration control. This may mean that actual thrust may not meet the desired control input, which may even make the system performance unstable. Therefore, the design of the composite controller must take into account the problem of actuator saturation.

$u_{\max}$ is assumed as the thruster's output maximum. In Section 4, the controller is designed as $\boldsymbol{u}=-\boldsymbol{b}\boldsymbol{F}_e-\hat{\boldsymbol{P}}_{J_2}+\boldsymbol{\tau}$, where $\boldsymbol{\tau}$=$\boldsymbol{K}\boldsymbol{e}$. Combined with the preceding conclusions, $\boldsymbol{u}$ is improved to form a saturation controller $\boldsymbol{u}_{\rm s}$ as

$$\boldsymbol{u}_{\rm s}=G(\boldsymbol{\tau}_{\rm s})=\begin{cases}\boldsymbol{\tau}_{\rm s}-\hat{\boldsymbol{P}}_{J_2}, & \|\boldsymbol{\tau}_{\rm s}\|\le u_{\max}-W_{J_2},\\ \mathrm{sign}(\boldsymbol{\tau}_{\rm s})\cdot(u_{\max}-W_{J_2}), & \|\boldsymbol{\tau}_{\rm s}\|>u_{\max}-W_{J_2}.\end{cases} \tag{20}$$

Based on the observer (14), setting $\boldsymbol{\tau}_{\rm s}=2\boldsymbol{K}\boldsymbol{e}$, and $\bar{\boldsymbol{u}}=\boldsymbol{u}_{\rm s}-\boldsymbol{\tau}_{\rm s}$ as control input, we can obtain

$$\begin{cases}\dot{\bar{\boldsymbol{X}}}=\bar{\boldsymbol{A}}\bar{\boldsymbol{X}}+\bar{\boldsymbol{B}}\boldsymbol{D}+\boldsymbol{B}_{\rm s}\bar{\boldsymbol{u}},\\ \bar{\boldsymbol{Z}}=\boldsymbol{C}\bar{\boldsymbol{X}}.\end{cases} \tag{21}$$

Theorem 2 Given σ_1>0, σ_2>0, and α>0, if there exist $\boldsymbol{Q}_1$>0, $\boldsymbol{P}_2$>0, $\boldsymbol{R}_1$, and $\boldsymbol{P}=\begin{bmatrix}\boldsymbol{P}_1 & 0\\ 0 & \boldsymbol{P}_2\end{bmatrix}=\begin{bmatrix}\boldsymbol{Q}_1^{-1} & 0\\ 0 & \boldsymbol{P}_2\end{bmatrix}$ satisfying

$$\boldsymbol{\Lambda}=\begin{bmatrix}\boldsymbol{P}\bar{\boldsymbol{A}}+\bar{\boldsymbol{A}}^{\rm T}\boldsymbol{P}^{\rm T} & \boldsymbol{P}\tilde{\boldsymbol{B}} & \tilde{\boldsymbol{C}}^{\rm T} & \boldsymbol{P}\bar{\boldsymbol{B}} & \boldsymbol{C}^{\rm T}\\ \tilde{\boldsymbol{B}}^{\rm T}\boldsymbol{P}^{\rm T} & -\boldsymbol{I} & \tilde{\boldsymbol{D}}^{\rm T} & 0 & 0\\ \tilde{\boldsymbol{C}} & \tilde{\boldsymbol{D}} & -\boldsymbol{I} & \tilde{\boldsymbol{E}} & 0\\ \bar{\boldsymbol{B}}^{\rm T}\boldsymbol{P}^{\rm T} & 0 & \tilde{\boldsymbol{E}}^{\rm T} & -\alpha^2\boldsymbol{I} & 0\\ \boldsymbol{C} & 0 & 0 & 0 & -\boldsymbol{I}\end{bmatrix}<0, \tag{22}$$

where

$$\tilde{\boldsymbol{B}}=[\sigma_1\boldsymbol{T}\quad \sigma_2\boldsymbol{B}_{\rm s}],\ \tilde{\boldsymbol{C}}=\begin{bmatrix}\boldsymbol{W}\bar{\boldsymbol{A}}/\sigma_1\\ \tilde{\boldsymbol{K}}/\sigma_2\end{bmatrix},$$

$$\tilde{\boldsymbol{D}}=\begin{bmatrix}0 & \sigma_2\boldsymbol{W}\boldsymbol{B}_{\rm s}/\sigma_1\\ 0 & 0\end{bmatrix},\ \tilde{\boldsymbol{E}}=[\boldsymbol{W}\bar{\boldsymbol{B}}/\sigma_1\quad 0]^{\rm T},$$

$$\tilde{\boldsymbol{K}}=[\boldsymbol{K}\quad 0],\ \boldsymbol{W}=[W_{J_2}\quad 0],$$

then the system (21) is uniformly ultimately bounded, and satisfies H_∞ performance $\|\bar{\boldsymbol{Z}}\|_2<\alpha\|\boldsymbol{D}\|_2$.

Proof Define the Lyapunov function as follows:

$$\boldsymbol{S}=\int_0^\infty\left[\boldsymbol{Z}^{\rm T}\boldsymbol{Z}-\alpha^2\boldsymbol{D}^{\rm T}\boldsymbol{D}+\dot{\bar{\boldsymbol{X}}}^{\rm T}\boldsymbol{P}\bar{\boldsymbol{X}}+\bar{\boldsymbol{X}}^{\rm T}\boldsymbol{P}\dot{\bar{\boldsymbol{X}}}+\frac{1}{\sigma_1^2}\left\|\boldsymbol{W}\dot{\bar{\boldsymbol{X}}}\right\|^2+\frac{1}{\sigma_2^2}\left(\left\|\tilde{\boldsymbol{K}}\bar{\boldsymbol{X}}\right\|^2-\|\boldsymbol{u}_{\rm s}\|^2\right)\right]{\rm d}t, \tag{23}$$

$$\begin{aligned}\dot{\boldsymbol{S}}&=\boldsymbol{Z}^{\rm T}\boldsymbol{Z}-\alpha^2\boldsymbol{D}^{\rm T}\boldsymbol{D}+\dot{V}\\ &=\bar{\boldsymbol{X}}^{\rm T}\boldsymbol{C}^{\rm T}\boldsymbol{C}\bar{\boldsymbol{X}}-\alpha^2\boldsymbol{D}^{\rm T}\boldsymbol{D}+\dot{\bar{\boldsymbol{X}}}^{\rm T}\boldsymbol{P}\bar{\boldsymbol{X}}+\bar{\boldsymbol{X}}^{\rm T}\boldsymbol{P}\dot{\bar{\boldsymbol{X}}}\\ &\quad+\frac{1}{\sigma_1^2}\left\|\boldsymbol{W}\dot{\bar{\boldsymbol{X}}}\right\|^2+\frac{1}{\sigma_2^2}\left(\left\|\tilde{\boldsymbol{K}}\bar{\boldsymbol{X}}\right\|^2-\|\boldsymbol{u}_{\rm s}\|^2\right)\\ &=\bar{\boldsymbol{X}}^{\rm T}\left(\boldsymbol{P}\bar{\boldsymbol{A}}+\bar{\boldsymbol{A}}^{\rm T}\boldsymbol{P}^{\rm T}+\frac{1}{\sigma_1^2}\bar{\boldsymbol{A}}^{\rm T}\boldsymbol{W}^{\rm T}\boldsymbol{W}\bar{\boldsymbol{A}}+\frac{1}{\sigma_2^2}\tilde{\boldsymbol{K}}^{\rm T}\tilde{\boldsymbol{K}}\right.\\ &\quad\left.+\boldsymbol{C}^{\rm T}\boldsymbol{C}\right)\bar{\boldsymbol{X}}+\boldsymbol{D}^{\rm T}\left(\frac{1}{\sigma_1^2}\bar{\boldsymbol{B}}^{\rm T}\boldsymbol{W}^{\rm T}\boldsymbol{W}\bar{\boldsymbol{B}}-\alpha^2\boldsymbol{I}\right)\boldsymbol{D}\\ &\quad+\begin{bmatrix}0 & \frac{1}{\sigma_2}\boldsymbol{u}_{\rm s}^{\rm T}\end{bmatrix}\begin{bmatrix}-\boldsymbol{I} & 0\\ 0 & \frac{\sigma_2^2}{\sigma_1^2}\boldsymbol{B}_{\rm s}^{\rm T}\boldsymbol{W}^{\rm T}\boldsymbol{W}\boldsymbol{B}_{\rm s}-\boldsymbol{I}\end{bmatrix}\begin{bmatrix}0\\ \frac{1}{\sigma_2}\boldsymbol{u}_{\rm s}\end{bmatrix}\end{aligned}$$

$$+\begin{bmatrix} 0 & \frac{1}{\sigma_2}\boldsymbol{u}_{\mathrm{s}}^{\mathrm{T}} \end{bmatrix}\begin{bmatrix} 0 \\ \frac{\sigma_2}{\sigma_1^2}\boldsymbol{B}_{\mathrm{s}}^{\mathrm{T}}\boldsymbol{W}^{\mathrm{T}}\boldsymbol{W}\bar{\boldsymbol{B}} \end{bmatrix}\boldsymbol{D}$$

$$+\boldsymbol{D}^{\mathrm{T}}\begin{bmatrix} 0 \\ \frac{\sigma_2}{\sigma_1^2}\boldsymbol{B}_{\mathrm{s}}^{\mathrm{T}}\boldsymbol{W}^{\mathrm{T}}\boldsymbol{W}\bar{\boldsymbol{B}} \end{bmatrix}^{\mathrm{T}}\begin{bmatrix} 0 \\ \frac{1}{\sigma_2}\boldsymbol{u}_{\mathrm{s}} \end{bmatrix}$$

$$+\bar{\boldsymbol{X}}^{\mathrm{T}}\begin{bmatrix} 0 & \sigma_2\boldsymbol{P}\boldsymbol{B}_{\mathrm{s}}+\frac{\sigma_2}{\sigma_1^2}\bar{\boldsymbol{A}}^{\mathrm{T}}\boldsymbol{W}^{\mathrm{T}}\boldsymbol{W}\boldsymbol{B}_{\mathrm{s}} \end{bmatrix}\begin{bmatrix} 0 \\ \frac{1}{\sigma_2}\boldsymbol{u}_{\mathrm{s}} \end{bmatrix}$$

$$+\begin{bmatrix} 0 & \frac{1}{\sigma_2}\boldsymbol{u}_{\mathrm{s}}^{\mathrm{T}} \end{bmatrix}\begin{bmatrix} 0 & \sigma_2\boldsymbol{P}\boldsymbol{B}_{\mathrm{s}}+\frac{\sigma_2}{\sigma_1^2}\bar{\boldsymbol{A}}^{\mathrm{T}}\boldsymbol{W}^{\mathrm{T}}\boldsymbol{W}\boldsymbol{B}_{\mathrm{s}} \end{bmatrix}^{\mathrm{T}}\bar{\boldsymbol{X}}$$

$$+\bar{\boldsymbol{X}}^{\mathrm{T}}\left(\boldsymbol{P}\bar{\boldsymbol{B}}+\frac{1}{\sigma_1^2}\bar{\boldsymbol{A}}^{\mathrm{T}}\boldsymbol{W}^{\mathrm{T}}\boldsymbol{W}\bar{\boldsymbol{B}}\right)\boldsymbol{D}$$

$$+\boldsymbol{D}^{\mathrm{T}}\left(\boldsymbol{P}\bar{\boldsymbol{B}}+\frac{1}{\sigma_1^2}\bar{\boldsymbol{A}}^{\mathrm{T}}\boldsymbol{W}^{\mathrm{T}}\boldsymbol{W}\bar{\boldsymbol{B}}\right)^{\mathrm{T}}\bar{\boldsymbol{X}}$$

$$=\boldsymbol{p}^{\mathrm{T}}\boldsymbol{\Lambda}_1\boldsymbol{p},$$

where

$$\boldsymbol{\Lambda}_1=\begin{bmatrix} \boldsymbol{P}\bar{\boldsymbol{A}}+\bar{\boldsymbol{A}}^{\mathrm{T}}\boldsymbol{P}^{\mathrm{T}}+\tilde{\boldsymbol{C}}^{\mathrm{T}}\tilde{\boldsymbol{C}}+\boldsymbol{C}^{\mathrm{T}}\boldsymbol{C} & \boldsymbol{P}\tilde{\boldsymbol{B}}+\tilde{\boldsymbol{C}}^{\mathrm{T}}\tilde{\boldsymbol{D}} & \boldsymbol{P}\bar{\boldsymbol{B}}+\tilde{\boldsymbol{C}}^{\mathrm{T}}\tilde{\boldsymbol{E}} \\ \tilde{\boldsymbol{B}}^{\mathrm{T}}\boldsymbol{P}^{\mathrm{T}}+\tilde{\boldsymbol{D}}^{\mathrm{T}}\tilde{\boldsymbol{C}} & \tilde{\boldsymbol{D}}^{\mathrm{T}}\tilde{\boldsymbol{D}}-\boldsymbol{I} & \tilde{\boldsymbol{D}}^{\mathrm{T}}\tilde{\boldsymbol{E}} \\ \bar{\boldsymbol{B}}^{\mathrm{T}}\boldsymbol{P}^{\mathrm{T}}+\tilde{\boldsymbol{E}}^{\mathrm{T}}\tilde{\boldsymbol{C}} & \tilde{\boldsymbol{E}}^{\mathrm{T}}\tilde{\boldsymbol{D}} & \tilde{\boldsymbol{E}}^{\mathrm{T}}\tilde{\boldsymbol{E}}-\alpha^2\boldsymbol{I} \end{bmatrix},$$

$$\boldsymbol{p}=\begin{bmatrix} \bar{\boldsymbol{X}}^{\mathrm{T}} & 0 & \boldsymbol{u}_{\mathrm{s}}^{\mathrm{T}}/\sigma_2 & \boldsymbol{D}^{\mathrm{T}} \end{bmatrix}.$$

Exchanging rows and columns of $\boldsymbol{\Lambda}_1$, it can be shown that $\boldsymbol{\Lambda}<0$ is equivalent to $\boldsymbol{\Lambda}_1<0$ according to the Schur supplementary lemma. Then if we substitute $\bar{\boldsymbol{A}}$, $\bar{\boldsymbol{B}}$, $\boldsymbol{C}$, $\boldsymbol{D}$, $\tilde{\boldsymbol{B}}$, $\tilde{\boldsymbol{C}}$, $\tilde{\boldsymbol{D}}$, $\tilde{\boldsymbol{E}}$, $\tilde{\boldsymbol{K}}$, $\boldsymbol{W}$ to $\boldsymbol{\Lambda}$, using matrix elementary transformation and multiplying the diagonal matrix diag$\{\boldsymbol{Q}_1, \boldsymbol{I}, \boldsymbol{I}, \boldsymbol{I}, \boldsymbol{I}, \boldsymbol{I}, \boldsymbol{I}, \boldsymbol{I}, \boldsymbol{I}\}$, Theorem 2 can be obtained (see the Appendix). $\boldsymbol{K}=\boldsymbol{R}_1\boldsymbol{Q}_1^{-1}$, $\boldsymbol{L}=\boldsymbol{P}_2^{-1}\boldsymbol{R}_2$, and Eq. (21) is uniformly ultimately bounded and satisfies $\|\bar{\boldsymbol{Z}}\|_2<\alpha\|\boldsymbol{D}\|_2$. The proof is completed.

6 Simulations

To demonstrate the efficiency of the proposed methods, LEO formation of three-satellite diversion was adopted as an example for numerical simulations in this study. To make the example similar to a real situation, very low eccentricity (<0.001) was still used as the initial element, but the equivalent influences could be ignored for flying-around formation control in this study, as shown by Canuto *et al.* (2011). The initial values of formation orbital parameters are given in Table 1.

Table 1 The initial values of formation orbital elements

Parameter	Value		
	Master	Slave 1	Slave 2
a	7.1356×10^6 m	7.1356×10^6 m	7.1356×10^6 m
e	0.00104761	0.00092569	0.00092569
i	98.4247°	98.4260°	98.4247°
Ω	220.2500°	220.2492°	220.2516°
ω	90.0000°	108.5471°	71.4530°

a: orbital radius; e: eccentricity; i: inclination; Ω: right ascension of the ascending node (RAAN); ω: argument of perigee

According to Theorem 2, we designed parameters as $\sigma_1=2$, $\sigma_2=3$, and $\alpha=20$. By solving Eq. (15), we obtained the parameter $\boldsymbol{K}$ of the state feedback controller and observer gain $\boldsymbol{L}$:

$$\boldsymbol{K}=\begin{bmatrix} -k_1 & k_2 & 0 & -k_3 & -k_4 & 0 \\ -k_2 & -k_1 & 0 & k_4 & -k_3 & 0 \\ 0 & 0 & -k_1 & 0 & 0 & -k_3 \end{bmatrix},$$

where $k_1=31.9832$, $k_2=0.0732$, $k_3=81.2185$, $k_4=0$,

$$\boldsymbol{L}=\begin{bmatrix} 0 & 0 & 0 & -1.7536 & -0.0000 & 0 \\ 0 & 0 & 0 & -0.0000 & -1.7536 & 0 \\ 0 & 0 & 0 & 0 & 0 & -1.7536 \end{bmatrix}.$$

First, we chose GPS (single point positioning error <1 m (spherical error probable, SEP)) as representative of GNSS to validate the relative navigation method in this paper. We assumed that every vehicle was equipped with one GPS receiver and that the relative attitude could not be determined, so only relative positioning was considered and simulated here. Through a nonlinear filter, the relative position errors converged rapidly to the order of 10^{-3} m, and the velocity to 10^{-4} m/s. Fig. 2 shows the Y_{r} axis relative position error, which was worse than those of the other two directions. The amplified section indicated that the error reached ±0.012 m. By plotting the relative position coordinates obtained from the positioning algorithm, the diversion trajectory (Fig. 3) was obtained.

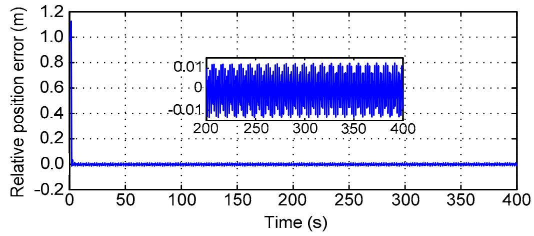

Fig. 2 Relative position error (Y_r axis) of formation navigation

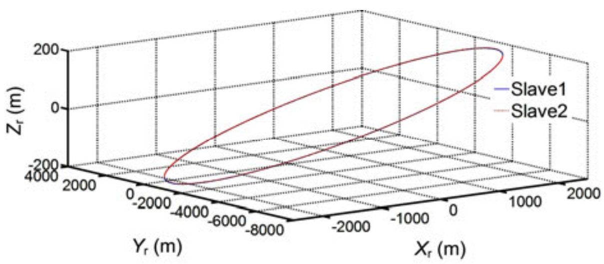

Fig. 3 Formation diversion trajectory calculated by relative positioning

Many control methods for formation configuration maintenance are used such as PID control and sliding mode control, but few of them aim to reject types of disturbances. In this section, to deal with this class of nonlinear formation system with various perturbations, the proposed composite controller was simulated. At the same time, an H_∞ control method similar to that adopted by Massioni *et al.* (2011) was compared with our presented method. Fig. 4 shows relative position maintenance errors using the composite control law. The errors decreased in hundreds of seconds regardless of the actuator's features. Fig. 5 shows that the designed disturbance observer can estimate the perturbation terms quickly and exactly.

Fig. 6 shows the Y_r axis comparison result using the common H_∞ controller (Sun *et al.*, 2004) and the composite disturbance attenuation controller. Clearly, our proposed method had higher precision, and the relative position errors were reduced by 60%–70% compared with conventional methods.

Nevertheless, all the simulation results above reveal the control effect without considering the saturation restriction, so the saturation controller was simulated here. We assumed that the control acceleration level was 10^{-6} m/s^2. Fig. 7 presents the position tracking errors, which converged slowly but less than 0.02 m from the partial enlarged details. Also, the control acceleration was kept below $\pm 2\times10^{-6}$ m/s^2. The screenshot (Fig. 8) shows the details of the control input signals for the micro thrust actuators. The actuators were assumed to have been installed symmetrically in three directions without noises, and the control signals were the total accelerations in the three directions.

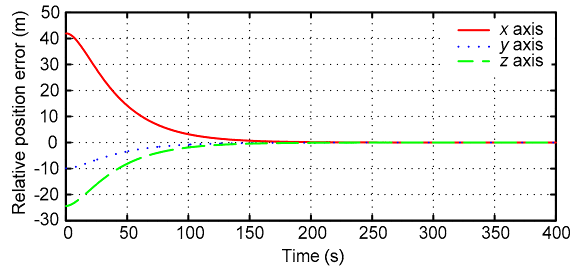

Fig. 4 Relative position tracking errors using the proposed controller

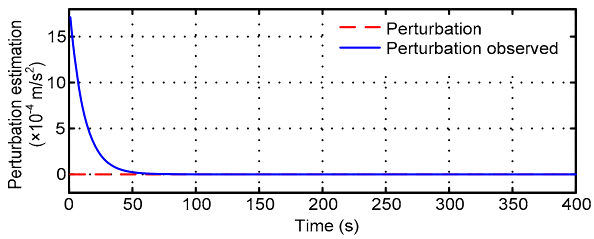

Fig. 5 P_{J_2} estimation (Y_r axis) using the observer

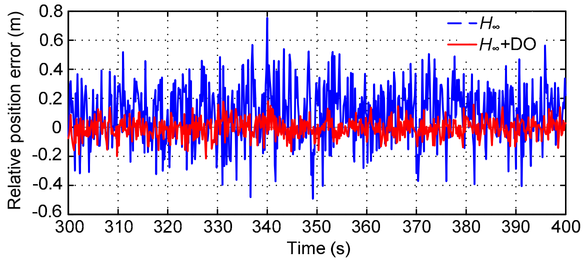

Fig. 6 Comparison of relative position errors (Y_r axis) between H_∞ and H_∞ with a disturbance observer (DO)

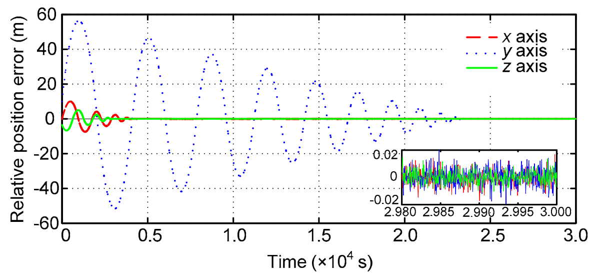

Fig. 7 Position tracking errors using the proposed saturation controller

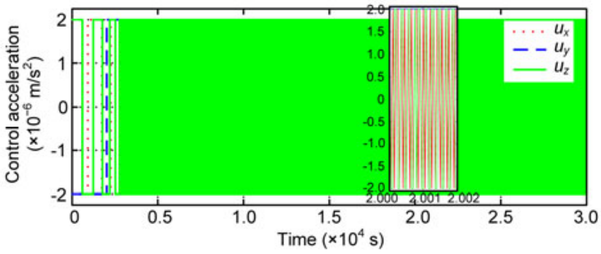

Fig. 8 Control acceleration of thrusters

7 Conclusions

In this paper, the nonlinear relative dynamics is constructed with analysis of primary perturbations for precise spacecraft formation missions. A feasible method is presented to classify the perturbations into different types of model disturbances, which contain slow variations and are norm bounded. Then, based on the dynamics equations above, a nonlinear filter is designed for accurate GNSS relative positioning. Utilizing the positioning results simultaneously, a composite disturbance attenuation controller is described to keep the configuration of the formation mission. The controller consists of DOBC combined with H_∞ state feedback with advantages of estimating and rejecting corresponding disturbances. For a better control effect, the saturated controller is designed under the condition of micro thrusters as actuators. By designing an appropriate Lyapunov function, the stability of the system is proved. Through numerical simulation, the GNSS relative positioning errors are reduced to within ±0.01 m. Also, the relative position error could be controlled within ±0.02 m while keeping the control acceleration less than 2×10^{-6} m/s^2. These results show that the system model, nonlinear filter, and composite controller are all able to meet the requirements of relative navigation and configuration maintenance for high performance formation missions.

Acknowledgements

This work was partially supported by Associate Prof. Pei-ling CUI and Associate Prof. Wei QUAN, Beihang University, China. The authors also gratefully acknowledge the helpful comments and suggestions of the anonymous reviewers.

References

Alfriend, K.T., Schaub, H., Gim, D.W., 2000. Gravitational Perturbations, Nonlinearity and Circular Orbit Assumption Effect on Formation Flying Control Strategies. American Astronautical Society Guidance & Control Conf., AAS 00-012, p.1-20.

Buist, P.J., Teunissen, P.J.G., Verhagen, S., Giorgi, G., 2011. A vectorial bootstrapping approach for integrated GNSS-based relative positioning and attitude determination of spacecraft. *Acta Astron.*, **68**(7-8):1113-1125. [doi:10.1016/j.actaastro.2010.09.027]

Canuto, E., 2007. Embedded model control: outline of the theory. *ISA Trans.*, **46**(3):363-377. [doi:10.1016/j.isatra.2007.01.006]

Canuto, E., Molano-Jimenez, A., Perez-Montenegro, C., Massotti, L., 2011. Long-distance, drag-free, low-thrust, LEO formation control for Earth gravity monitoring. *Acta Astron.*, **69**(7-8):571-582. [doi:10.1016/j.actaastro.2011.04.018]

Clohessy, W.H., Wiltshire, R.S., 1960. Terminal guidance system for satellite rendezvous. *J. Aerosp. Sci.*, **27**(9):653-658.

de Souza, C.E., Xie, L., 1992. On the discrete-time bounded real lemma with application in the characterization of static state feedback H_∞ controllers. *Syst. Control Lett.*, **18**(1):61-71. [doi:10.1016/0167-6911(92)90108-5]

Fang, J.C., Gong, X.L., 2010. Predictive iterated Kalman filter for INS/GPS integration and its application to SAR motion compensation. *IEEE Trans. Instrum. Meas.*, **59**(4): 909-915. [doi:10.1109/TIM.2009.2026614]

Guo, L., Chen, W.H., 2005. Disturbance attenuation and rejection for systems with nonlinearity via DOBC approach. *Int. J. Rob. Nonl. Control*, **15**(3):109-125. [doi:10.1002/rnc.978]

Guo, L., Feng, C.B., Chen, W.H., 2006. A survey of disturbance-observer-based control for dynamic nonlinear system. *Dynam. Cont. Discr. Impul. Syst.*, **13**:79-84.

Han, K., Hao, W., Jin, Z.H., 2010. Magnetometer-only linear attitude estimation for bias momentum pico-satellite. *J. Zhejiang Univ.-Sci. A (Appl. Phys. & Eng.)*, **11**(6):455-464. [doi:10.1631/jzus.A0900725]

Massioni, P., Keviczky, T., Gill, E., Verhaegen, M., 2011. A decomposition-based approach to linear time-periodic distributed control of satellite formations. *IEEE Trans. Control Syst. Technol.*, **19**(3):481-492. [doi:10.1109/TCST.2010.2051228]

Schaub, H., Vadali, S.R., Junkins, J.L., Alfriend, K.T., 2000. Spacecraft formation flying control using mean orbit elements. *J. Astron. Sci.*, **48**(1):69-87.

Sun, D., Zhou, F.Q., Zhou, J., 2004. Robust control for multiple spacecraft flying. *J. Proj. Rock. Miss. Guid.*, **24**(2): 279-281.

Vaddi, S.S., Vadali, S.R., Alfriend, K.T., 2003. Formation flying: accommodating nonlinearity and eccentricity perturbations. *J. Guid. Control Dyn.*, **26**(2):214-223. [doi:10.2514/2.5054]

Wang, Z.K., Zhang, Y.L., 2007. Design and verification of a

robust formation keeping controller. *Acta Astron.*, **61**(7-8):565-574. [doi:10.1016/j.actaastro.2007.01.064]
Winternitz, L.M.B., Bamford, W.A., Heckler, G.W., 2009. A GPS receiver for high-altitude satellite navigation. *IEEE J. Sel. Top. Signal Process.*, **3**(4):541-556. [doi:10.1109/JSTSP.2009.2023352]
Wnuk, E., Golebiewska, J., 2007. Relative satellite motion in a formation. *Adv. Space Res.*, **40**(1):35-42. [doi:10.1016/j.asr.2007.01.049]
Xu, G.Y., Wang, D.W., 2008. Nonlinear dynamic equations of satellite relative motion around an oblate Earth. *J. Guid. Control Dyn.*, **31**(5):1521-1524. [doi:10.2514/1.33616]
Yoon, S., Lundberg, J.B., 2001. Euler angle dilution of precision in GPS attitude determination. *IEEE Trans. Aerosp. Electron. Syst.*, **37**(3):1077-1083. [doi:10.1109/7.953258]
You, Z.H., Li, B., Dong, Z.H., 2005. Status and key technologies of spacecraft formation on Sun-Earth Lagrange point. *Aerosp. China*, **5**(7):27-31 (in Chinese).
Zhang, J.X., Cao, X.B., Wang, J.H., Lin, X.H., 2009. Configuration, orbit design of InSAR formation based on mean elements. *IEEE Trans. Aerosp. Electron. Syst.*, **45**(2):747-752. [doi:10.1109/TAES.2009.5089555]
Zhang, Y.L., Zeng, G.Q., Wang, Z.K., 2008. Theories and Applications of Distributed Satellites System. Science Publishing Company, Beijing (in Chinese).

Appendix: Proof of Theorem 2

As denoted, $\boldsymbol{P}=\begin{bmatrix}\boldsymbol{P}_1 & 0\\ 0 & \boldsymbol{P}_2\end{bmatrix}=\begin{bmatrix}\boldsymbol{Q}_1^{-1} & 0\\ 0 & \boldsymbol{P}_2\end{bmatrix}$, substituting $\bar{\boldsymbol{A}}$, $\bar{\boldsymbol{B}}$, $\boldsymbol{C}$, $\boldsymbol{D}$, $\tilde{\boldsymbol{B}}$, $\tilde{\boldsymbol{C}}$, $\tilde{\boldsymbol{D}}$, $\tilde{\boldsymbol{E}}$, $\tilde{\boldsymbol{K}}$, $\boldsymbol{W}$ to $\boldsymbol{\Lambda}$ with matrix elementary transformation, we can obtain

$$\boldsymbol{\Lambda}=\begin{bmatrix}\boldsymbol{\Lambda}_{\rm a} & \boldsymbol{\Lambda}_{\rm b}\end{bmatrix}<0, \tag{A1}$$

where

$$\boldsymbol{\Lambda}_{\rm a}=\begin{bmatrix}
\boldsymbol{\Lambda}_{11} & 0 & \sigma_2\boldsymbol{P}_1\boldsymbol{B}_{\rm u} & \boldsymbol{\Lambda}_{14} & \frac{1}{\sigma_2}\boldsymbol{K}^{\rm T}\\
\frac{1}{\sigma_2}\boldsymbol{K}^{\rm T} & -\boldsymbol{I} & 0 & 0 & 0\\
* & * & -\boldsymbol{I} & \frac{\sigma_2}{\sigma_1}(\boldsymbol{W}_{J_2}\boldsymbol{B}_{\rm u})^{\rm T} & 0\\
* & * & * & -\boldsymbol{I} & 0\\
* & * & * & * & -\boldsymbol{I}\\
* & * & * & * & *\\
* & * & * & * & *\\
* & * & * & * & *\\
* & * & * & * & *
\end{bmatrix},$$

$$\boldsymbol{\Lambda}_{\rm b}=\begin{bmatrix}
0 & \boldsymbol{P}_1\boldsymbol{B}_{\rm ad} & \boldsymbol{C}_1^{\rm T} & \boldsymbol{P}_1\boldsymbol{B}_{J_2}\\
0 & 0 & 0 & 0\\
0 & 0 & 0 & 0\\
0 & \frac{1}{\sigma_1}\boldsymbol{W}_{J_2}\boldsymbol{B}_{\rm ad} & 0 & \boldsymbol{\Lambda}_{49}\\
0 & 0 & 0 & 0\\
-\alpha^2\boldsymbol{I} & 0 & 0 & \boldsymbol{P}_2^{\rm T}\\
* & -\alpha^2\boldsymbol{I} & 0 & \boldsymbol{\Lambda}_{79}\\
* & * & -\boldsymbol{I} & \boldsymbol{C}_2\\
* & * & * & \boldsymbol{\Lambda}_{99}
\end{bmatrix},$$

where ‘*’ denotes symmetric terms of a symmetric matrix, and

$$\begin{aligned}
\boldsymbol{\Lambda}_{11}&=\mathrm{sym}(\boldsymbol{P}_1(\boldsymbol{A}+\boldsymbol{B}_{\rm u}\boldsymbol{K})),\\
\boldsymbol{\Lambda}_{14}&=[\boldsymbol{W}_{J_2}(\boldsymbol{A}+\boldsymbol{B}_{\rm u}\boldsymbol{K})]^{\rm T}/\sigma_1,\\
\boldsymbol{\Lambda}_{49}&=[(\boldsymbol{W}_{J_2}\boldsymbol{B}_{J_2})^{\rm T}/\sigma_1]^{\rm T},\\
\boldsymbol{\Lambda}_{79}&=-(\boldsymbol{P}_2\boldsymbol{L}\boldsymbol{B}_{\rm ad})^{\rm T},\\
\boldsymbol{\Lambda}_{99}&=-\mathrm{sym}(\boldsymbol{P}_2\boldsymbol{L}\boldsymbol{W}_{J_2}).
\end{aligned}$$

Pre- and post-multiplying inequality (A1) by diag$\{\boldsymbol{Q}_1$, $\boldsymbol{I}, \boldsymbol{I}, \boldsymbol{I}, \boldsymbol{I}, \boldsymbol{I}, \boldsymbol{I}, \boldsymbol{I}\}$, inequality (A2) can be obtained:

$$\boldsymbol{\Theta}=\begin{bmatrix}\boldsymbol{\Theta}_{\rm a} & \boldsymbol{\Theta}_{\rm b}\end{bmatrix}<0, \tag{A2}$$

where

$$\boldsymbol{\Theta}_{\rm a}=\begin{bmatrix}
\boldsymbol{\Theta}_{11} & 0 & \sigma_2\boldsymbol{B}_{\rm u} & \boldsymbol{\Theta}_{14} & \frac{1}{\sigma_2}\boldsymbol{R}_1^{\rm T}\\
* & -\boldsymbol{I} & 0 & 0 & 0\\
* & * & -\boldsymbol{I} & \frac{\sigma_2}{\sigma_1}\boldsymbol{W}_{J_2}\boldsymbol{B}_{\rm u}^{\rm T} & 0\\
* & * & * & -\boldsymbol{I} & 0\\
* & * & * & * & -\boldsymbol{I}\\
* & * & * & * & *\\
* & * & * & * & *\\
* & * & * & * & *\\
* & * & * & * & *
\end{bmatrix},$$

$$
\boldsymbol{\Theta}_{\mathrm{b}}=\begin{bmatrix}
0 & \boldsymbol{B}_{\mathrm{ad}} & \boldsymbol{Q}_1\boldsymbol{C}_1^{\mathrm{T}} & \boldsymbol{B}_{J_2}\\
0 & 0 & 0 & 0\\
0 & 0 & 0 & 0\\
0 & \frac{1}{\sigma_1}\boldsymbol{W}_{J_2}\boldsymbol{B}_{\mathrm{ad}} & 0 & \frac{1}{\sigma_1}\boldsymbol{W}_{J_2}\boldsymbol{B}_{J_2}\\
0 & 0 & 0 & 0\\
-\alpha^2\boldsymbol{I} & 0 & 0 & \boldsymbol{P}_2\\
* & -\alpha^2\boldsymbol{I} & 0 & -\boldsymbol{B}_{\mathrm{ad}}^{\mathrm{T}}\boldsymbol{R}_2^{\mathrm{T}}\\
* & * & -\boldsymbol{I} & \boldsymbol{C}_2\\
* & * & * & -\mathrm{sym}(\boldsymbol{R}_2\boldsymbol{B}_{J_2})
\end{bmatrix},
$$

$$\boldsymbol{\Theta}_{11}=\mathrm{sym}(\boldsymbol{A}\boldsymbol{Q}_1+\boldsymbol{B}_{\mathrm{u}}\boldsymbol{R}_1),$$

$$\boldsymbol{\Theta}_{14}=\frac{1}{\sigma_1}(\boldsymbol{A}\boldsymbol{Q}_1+\boldsymbol{B}_{\mathrm{u}}\boldsymbol{R}_1)^{\mathrm{T}}\boldsymbol{W}_{J_2}{}^{\mathrm{T}},$$

$$\boldsymbol{R}_1=\boldsymbol{K}\boldsymbol{Q}_1,\quad \boldsymbol{R}_2=\boldsymbol{P}_2\boldsymbol{L}.$$

Recommended reading

Li, J.F., Meng, X., Gao, Y.F., Li, X., 2005. Study on relative orbital configuration in satellite formation flying. *Acta Mech. Sin.*, **21**(1):87-94. [doi:10.1007/s10409-004-0009-3]

Liu, H.P., Sun, F.C., Hu, Y.N., 2005. H-infinity control for fuzzy singularly perturbed systems. *Fuzzy Sets Syst.*, **155**(2):272-291. [doi:10.1016/j.fss.2005.05.004]

Liu, H.P., Sun, F.C., Sun, Z.Q., 2005. Stability analysis and synthesis of fuzzy singularly perturbed systems. *IEEE Trans. Fuzzy Syst.*, **13**(2):273-284. [doi:10.1109/TFUZZ.2004.839660]

Schweighart, S.A., Sedwick, R.J., 2005. Cross-track of satellite formations in the presence of J2 disturbances. *J. Guid. Control Dyn.*, **28**(4):824-826. [doi:10.2514/1.12387]

Xiong, K., Zhang, H., Liu, L., 2008. Adaptive robust extended Kalman filter for nonlinear stochastic systems. *IET Control Theory Appl.*, **2**(3):239-250. [doi:10.1049/iet-cta:20070096]
